Proceedings Paper:
Mortimer, L, Fairweather, M and Njobuenwu, DO orcid.org/0000-0001-6606-1912 (2017) Particle concentration and stokes number effects in multi-phase turbulent channel flows. In: Particles 2017: V International Conference on Particle-based Methods. Fundamentals and Applications. 5th International Conference on Particle-Based Methods (Particles 2017), 26-28 Sep 2017, Hannover, Germany. International Center for Numerical Methods in Engineering , pp. 859-869. ISBN 9788494690976

PARTICLE CONCENTRATION AND STOKES NUMBER EFFECTS IN MULTI-PHASE TURBULENT CHANNEL FLOWS

L. MORTIMER, M. FAIRWEATHER AND D. O. NJOBUENWU

University of Leeds
School of Chemical and Process Engineering, University of Leeds, Leeds, LS2 9JT, UK
pmlfm@leeds.ac.uk

Key words: Direct numerical simulation, Lagrangian particle tracking, Particle-laden flow, Fluid dynamics, Concentration, Stokes number

Abstract. This investigation examines the effect that particle concentration has on the dynamics of two-phase turbulent channel flows at low and high density ratios. In the literature, little explanation is offered for the existence of high particle turbulence intensities in the buffer layer and viscous sublayer for particles with high Stokes number. The present study aims to explore particle dynamics in those regions. The spectral element method DNS solver, Nek5000, is used to model the fluid phase at a shear Reynolds number, $Re_\tau = 180$. Particles are tracked using a Lagrangian approach with inter-phase momentum exchange (two-way coupling). Mean fluid and particle velocity statistics are gathered and analysed to determine the effect of increasing both Stokes number and concentration. Results indicate that the system with the greater Stokes number (air) has a much larger impact on the mean streamwise velocity and turbulence intensity profiles. As the concentration is increased, the mean flow velocity and turbulence intensity are reduced in the bulk and increased very close to the wall. For the low Stokes system, there is negligible effect on the flow statistics at low concentration. One-way coupled solid-phase statistics indicate that particles in water follow the flow very closely. At the higher density-ratio, particles lag behind the flow in the bulk, but overtake the flow in the near-wall region, where the existence of increased streamwise turbulence intensities is also observed. To elucidate the dynamics, concentrations and fluxes are analysed. Particles are observed to be distributed more densely close to the wall in air, compared to a reasonably uniform distribution in water. Finally, contour plots indicate that particles in air tend to congregate in regions of low streamwise fluid velocity, and the extent to which this differs between the two systems is then quantitatively measured.

1 INTRODUCTION

The transport of solid particles by turbulent fluid flows is common in many natural and industrial processes. A detailed understanding of the dynamics of such systems is important in determining the properties of the flow, and in particular the dispersion, deposition and resuspension of particles. A knowledge of these mechanisms is vital to improving and optimising flow systems containing particulate suspensions. Nevertheless, due to the complex nature of particle-turbulence interaction, the dynamics and mechanisms underpinning the motion of particles in these flows is currently not fully understood. Previous work investigating this kind of phenomena has demonstrated Stokes number-dependent particle behaviour in the near-wall region [1-3]. However, understanding of the physics of this behaviour is poor, with

relatively few sources offering explanations for its existence. Preferential concentration of particles in low-velocity regions close to solid surfaces has also been observed [4], but the extent to which particles remain in these low speed streaks is unknown. The topic of turbulence modulation through two-way coupling is also of great interest, since the volume fraction of most industrial flows tends to be high. It has been shown that the addition of particles can either enhance or attenuate the turbulence depending on the properties of the solid phase [5]. This tends to depend on the size of the particles such that those with large diameters ($d_P > 500\mu m$) will increase the streamwise turbulence intensity [6] whilst the latter is attenuated for those with small diameters.

The purpose of this study is to compare the dispersive properties of particle-laden turbulent flows at two different Stokes numbers representing identical glass particles in water and air. By fixing the diameter of each set of particles, we can examine more closely the effect of density ratio. In order to assess the extent to which particle concentration affects the turbulence field, the air channel flow is also compared at low and high volume fractions.

The fluid phase is modelled using the direct numerical simulation code, Nek5000, at a shear Reynolds number, $Re_\tau = 180$. A two-way coupled Lagrangian point-particle tracking method is used to predict the dispersed solid phase. A non-dimensional particle equation of motion is introduced using solely solid phase properties, non-dimensionalised against bulk fluid length and timescales. This includes the effects of drag, lift, pressure gradient and added mass forces. A feedback force is included in the Navier-Stokes equations based on the sum of particle forces in a grid-cell to account for two-way coupling. In both low and high concentration situations, the volume fraction is high enough to cause turbulence modulation. To allow focus primarily on the two-way interaction of these systems, inter-particle collisions will not be considered.

2 METHODOLOGY

2.1 Fluid simulation

The carrier-fluid field representing a fully developed channel flow is obtained using direct numerical simulation. This allows for resolution of the smallest length and time scales associated with the dynamic turbulent structures of the flow. In this work the Eulerian-phase solver, Nek5000 [7], was used which utilizes a high-order spectral element method to simulate the fluid phase. This code was chosen due to its efficient parallelisation capabilities and extensive testing and validation history. In the code, the incompressible Navier-Stokes equations are solved to high accuracy on a discretized Cartesian grid consisting of $27 \times 18 \times 23$ 8^{th} order elements (i.e. 5.7M nodes). The elements are scaled such that the nodes closest to the wall are distributed more densely. The Navier-Stokes equations are non-dimensionalised using the channel half-height, δ, the bulk velocity, U_B, and the fluid phase density, ρ_F. From here on, a quantity with an asterisk (*) denotes a variable non-dimensionalised in this manner.

The equations are:

$$\boldsymbol{\nabla} \cdot \boldsymbol{u}^* = 0 \tag{1}$$

$$\frac{\partial \boldsymbol{u}^*}{\partial t^*} + \boldsymbol{u}^* \cdot \boldsymbol{\nabla} \boldsymbol{u}^* = -\boldsymbol{\nabla} \mathrm{p}^* + \frac{1}{Re_B} \boldsymbol{\nabla} \cdot \boldsymbol{\tau}^* + \boldsymbol{f}_C^* \tag{2}$$

where $\boldsymbol{u}^*$ is the fluid velocity, p^* is the fluid pressure, Re_B is the bulk Reynolds number defined

as $Re_B = U_B\delta/\nu_F$, ν_F is the fluid kinematic viscosity and $\boldsymbol{\tau}^*$ is the viscous stress tensor. The additional term $\boldsymbol{f}_C^*$ is cell-dependent and accounts for the two-way momentum exchange between particles in that cell and the surrounding fluid.

For this study, the computational position domain (x, y, z) corresponds to a $12\delta \times 2\delta \times 6\delta$ channel. Here, x is the streamwise direction, y is the wall-normal direction, and z is the spanwise direction. Periodic boundary conditions are enforced in the streamwise and spanwise directions, whereas the wall-normal axis uses nonslip conditions at $y^* = \pm\delta$. The flow is driven and maintained by a constant pressure gradient. Using non-dimensional parameters this is:

$$\frac{\partial p^*}{\partial x^*} = \left(\frac{Re_\tau}{Re_B}\right)^2 \tag{3}$$

where Re_τ is the shear Reynolds number.

2.2 Particle dynamics

In order to model the transport of large numbers of particles through the fluid field, a Lagrangian particle tracker (LPT) was developed which interfaces concurrently with Nek5000. Each element of the solid phase is represented by a computational sphere. The LPT solves the non-dimensional Newtonian equations of motion for each particle in order to calculate trajectories. This equation is derived by considering the force-balance between the particle's inertia and the fluid. For this study, we have chosen to consider contributions from drag, lift, virtual mass and pressure gradient forces. The Basset history force has been neglected due to long computation times and previous evidence [8] showing little effect on the resulting motion.

The equations of motion are as follows:

$$\frac{\partial \boldsymbol{x}_{\boldsymbol{P}}^*}{\partial t^*} = \boldsymbol{u}_{\boldsymbol{P}}^* \tag{4}$$

$$\frac{\partial \boldsymbol{u}_{\boldsymbol{P}}^*}{\partial t^*} = \underbrace{\frac{3C_D|\mathbf{u}_\mathbf{S}^*|}{4d_p^*\rho_P^*}\mathbf{u}_\mathbf{S}^*}_{Drag} + \underbrace{\mathbf{g}^*(1-\rho^*)}_{Gravity} + \underbrace{\frac{3}{4}\frac{C_L}{\rho_P^*}(\mathbf{u}_\mathbf{S}^* \times \boldsymbol{\omega}_F^*)}_{Lift} + \underbrace{\frac{1}{2\rho_P^*}\frac{D'\mathbf{u}_\mathbf{F}^*}{Dt^*}}_{Virtual\ Mass} + \underbrace{\frac{1}{\rho_P^*}\frac{D\mathbf{u}_\mathbf{F}^*}{Dt^*}}_{Pressure\ Gradient} \tag{5}$$

In Equations (4) and (5), $\boldsymbol{x}_{\boldsymbol{P}}^*$ represents the coordinates of the particle position, $\boldsymbol{u}_{\boldsymbol{P}}^*$ is the particle velocity, $\boldsymbol{u}_{\boldsymbol{S}}^* = \boldsymbol{u}_{\boldsymbol{F}}^* - \boldsymbol{u}_{\boldsymbol{P}}^*$ is the particle-fluid slip velocity, d_P^* is the diameter of the particle non-dimensionalised by the channel half-height, ρ_P^* is the particle-fluid density ratio and $\boldsymbol{\omega}_{\boldsymbol{F}}^*$ is the fluid vorticity at the particle position given by $\boldsymbol{\omega}_{\boldsymbol{F}}^* = \boldsymbol{\nabla} \times \boldsymbol{u}_{\boldsymbol{F}}^*$. The drag coefficient, C_D, is taken from standard empirical observations [9, 10] and the lift term uses the Saffman-Mei [11, 12] coefficient. A fourth order accuracy Runge-Kutta scheme was applied (with a Δt equal to that of the continuous phase solver) for integration of the differential equations in order to obtain each particle's position and velocity at each fluid timestep. Each particle's inertial effect on the fluid phase was considered through the inclusion of an additional source term in the Navier-Stokes equations:

$$\boldsymbol{f}_C^* = \frac{1}{V_C}\sum_{P=1}^{N_P} \boldsymbol{F}_{\boldsymbol{P}}^* \tag{6}$$

where V_C is the volume of a computational cell, N_P is the number of particles in that cell and $\boldsymbol{F}_{\boldsymbol{P}}^*$ is the non-dimensional fluid force exerted on particle P. This is applied at each fluid timestep

and uses the particle force calculation from the previous timestep.

Table 1: Simulation parameters (L: Low concentration, H: High concentration).

Parameter	Water (L)	Air (L)	Water (H)	Air (H)
Shear Reynolds number, Re_τ	180	180	180	180
Bulk Reynolds number, Re_B	2800	2800	2800	2800
Particle diameter, d_P^*	0.005	0.005	0.005	0.005
Number of particles, N_P	300,000	300,000	2,566,851	2,566,851
Shear Stokes number, St_τ	0.113	91.845	0.113	91.845
Bulk Stokes number, St_B	0.01	7.937	0.01	7.937
Density ratio, ρ_P^*	2.5	2041	2.5	2041
Volume fraction, Θ_P	10^{-4}	10^{-4}	10^{-3}	10^{-3}

The properties used in each simulation are presented in Table 1. Each simulation presented here was performed both one-way and two-way coupled, with the exception of the high-concentration water flow due to time constraints. The simulations were first run as a single-phase flow using a standard turbulent profile with added chaotic terms in the wall-normal and spanwise directions. Once turbulence was established, fluid statistics were monitored every 100 non-dimensional time units until the mean streamwise velocity and RMS velocity fluctuations had reached a statistically steady state.

Particles were then injected uniformly throughout the channel and given an initial velocity equal to that of the fluid. Particle statistical distributions across the wall-normal direction were obtained by splitting the domain into 120 cuboidal regions of equal size, and taking an average over all the particles in that zone. Once the particle number density near the wall had reached a stable value, considered later, particle data was collected and statistics were obtained. It was from this stable state that the two-way coupled runs were started, reducing the fluid and particle timestep initially to avoid divergences in the flow field due to high particle forces. The fluid velocity statistics were then tracked once again to determine whether the system had finished responding to the addition of momentum-coupling. Once satisfied, statistics were reobtained as previously.

3 RESULTS AND DISCUSSION

3.1 Fluid phase statistics

This section explores the effect of particle concentration and Stokes number on the dynamics of the fluid phase. All flow variables plotted here are normalised by the bulk properties of the flow. Figure 1 compares the mean streamwise velocity of the fluid for each simulation as well as for the unladen flow. Here, the difference between the unladen flow and the low concentration two-phase flow in water is negligible. This is due to the low Stokes number, limiting the momentum coupling between the two phases. In the low concentration air simulation, the mean velocity profile is slightly reduced in the bulk flow region.

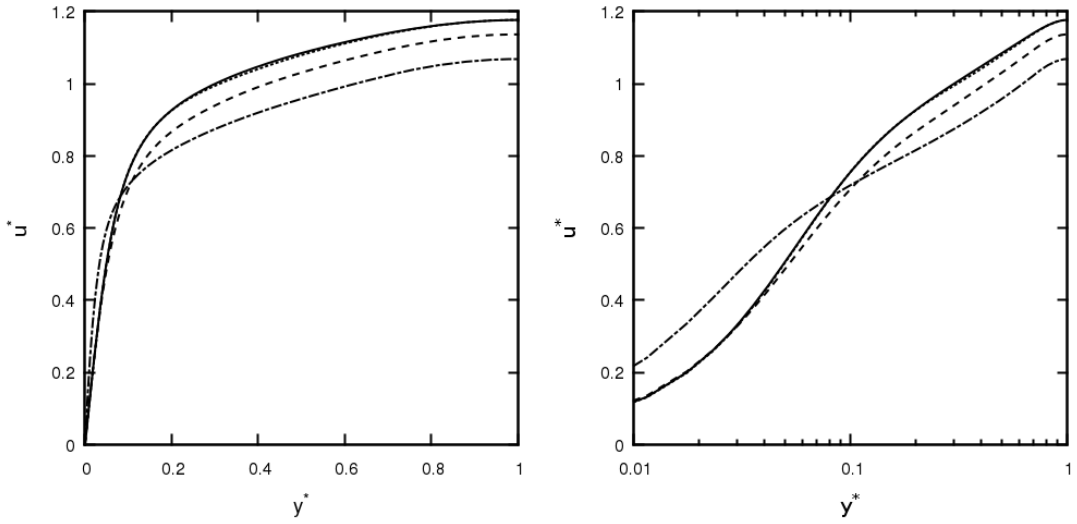

Figure 1: Mean streamwise fluid velocity comparison. —— : unladen flow; - - - : two-way coupled air phase at low concentration; ..... : two-way coupled water phase at low concentration; – · – : two-way coupled air phase at high concentration.

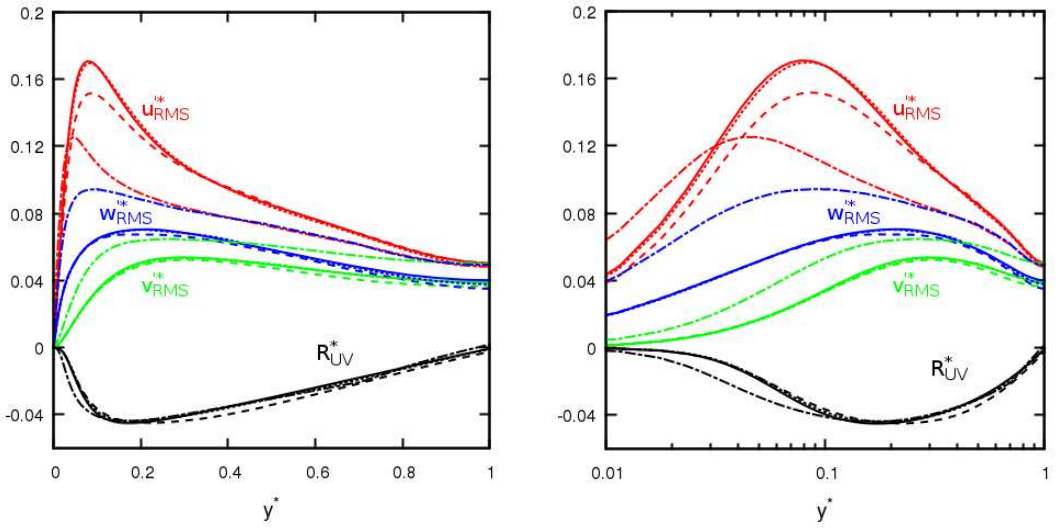

Figure 2: RMS fluid velocity fluctuations and shear stress comparison. —— : unladen flow; - - - : two-way coupled air phase at low concentration; ..... : two-way coupled water phase at low concentration; – · – : two-way coupled air phase at high concentration.

This is further emphasised at high concentration, with an increase in fluid velocity found near the wall. This effectively reduces the thickness of the boundary layer and increases the wall shear stress due to a higher wall-normal velocity derivative. The combination of both increased volume fraction and density ratio provides the particle phase with enough inertia to increase the fluid velocity close to the wall.

The fluid phase turbulent normal and shear stresses are presented in Figure 2. When

compared to the unladen flow (solid lines), the particles once again show negligible impact on the water phase. With increased volume fraction, particles tend to reduce the streamwise turbulence intensities and increase the wall-normal and spanwise components. Close attention to the rightmost graph in Figure 2 indicates that the streamwise turbulence intensities are increased very close to the wall at $y^* < 0.035$.

3.2 Particle phase statistics

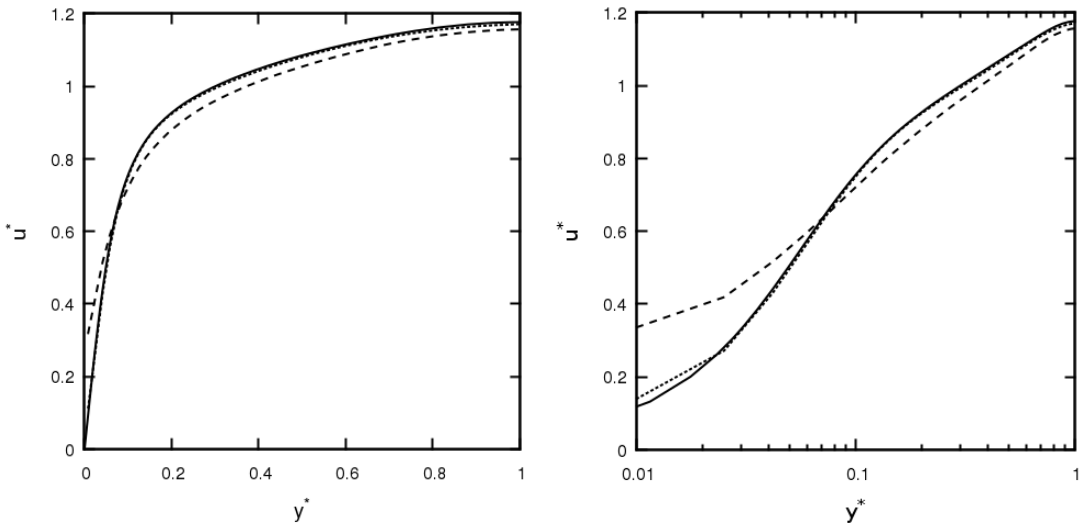

Figure 3: Mean streamwise particle velocity comparison. ——— : unladen flow; - - - : one-way coupled particle phase at high concentration in air; ..... : one-way coupled particle phase at high concentration in water;

To explore the dynamics associated with the particle phase, mean velocity and RMS velocity fluctuation statistics were obtained. Figure 3 compares the one-way coupled particle mean velocities in the streamwise direction. Since one-way coupled flow statistics are concentration-independent, only the high concentration systems are considered here. For water, the particle profile is very similar to the fluid profile, with a slight increase towards the wall at $y^* < 0.02$. Particles in air generally lag behind the fluid in the bulk region, but travel faster than the fluid at $y^* < 0.08$.

Particle RMS velocities are plotted in Figure 4. There are slight deviations from all three fluid RMS components in the water channel. The spanwise and wall-normal components are all reduced slightly when compared to the unladen flow, which is most emphasised around $y^* = 0.2$ (i.e. on the boundary between the bulk and log-law regions). The streamwise component resides very close to the unladen flow except for very close to the wall where it increases somewhat. These effects are strongly emphasised at the higher Stokes number (air). A very notable feature is that the streamwise RMS velocity increases as the wall is approached and is significantly larger than for the unladen flow profile. Large RMS values imply that particle slip velocities will also be high, since the particles are unlikely to be following the flow directly in that region due to their range of speeds. This is then directly linked to the magnitude of the coupling in that region, since the predominant forces (drag and lift) will be much greater. In

this case it seems that the particles dampen the momentum, moving in a more turbulent manner themselves. In the spanwise and wall-normal direction, particles possess enough inertia to avoid being influenced by the fluid turbulence, and so their RMS velocity profiles are greatly reduced.

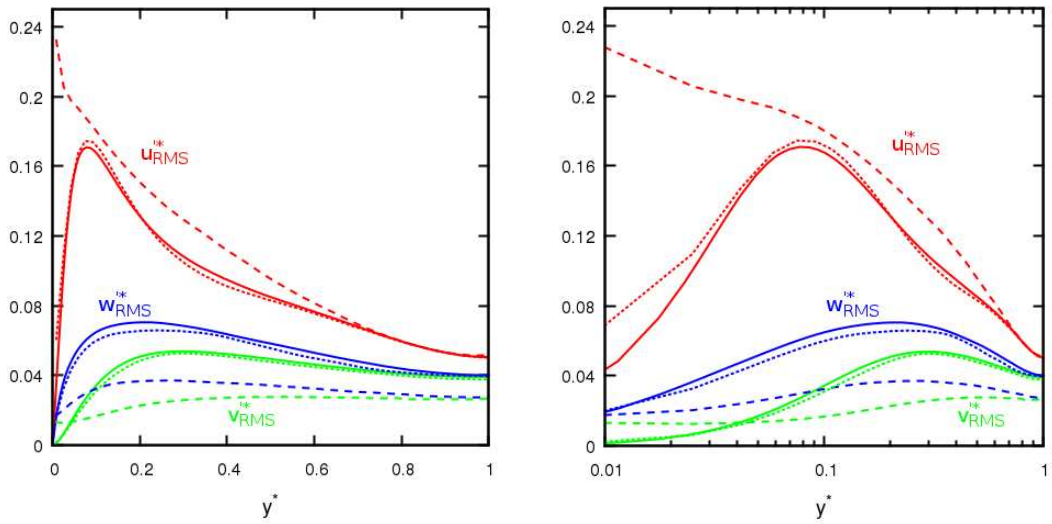

Figure 4: RMS particle velocity fluctuations comparison. —— : unladen flow; - - - : one-way coupled particle phase at high concentration in air; ..... : one-way coupled particle phase at high concentration in water;

The left plot in Figure 5 depicts the concentration of particles close to the wall over time which is used to establish whether the particle motion has reached stability. The concentration is normalised by the concentration at injection. Clearly particles in air take around 30 non-dimensional time units to reach this point, after which the gradient drops off greatly and the normalised concentration continues to deviate slightly around 2.7. The right plot shows the distribution of particles across the channel at $t^* = 150$. Here we can see more directly the effects of the increase in wall-region particle concentration for the air channel. The water channel profile remains very flat, aside from a slight increase and dip very close to the wall.

Table 2 defines the boundaries of the regions of the flow and provides the mean net flux of particles through those regions per timestep both up (towards the centre-line) and down (towards the wall). For water, it is evident that the flux (upwards and downwards) through each plane separating two regions is almost identical. This implies that there is no net 'flow' of particles in any particular direction, which is further validated by the right plot of Figure 5. This also seems to be true for air, however, there are far fewer particles moving between the log-law region and the buffer layer than there are in water. Conversely, there are more particles moving between the buffer layer and the viscous sublayer than there are in water, indicating more wall-normal motion in that region.

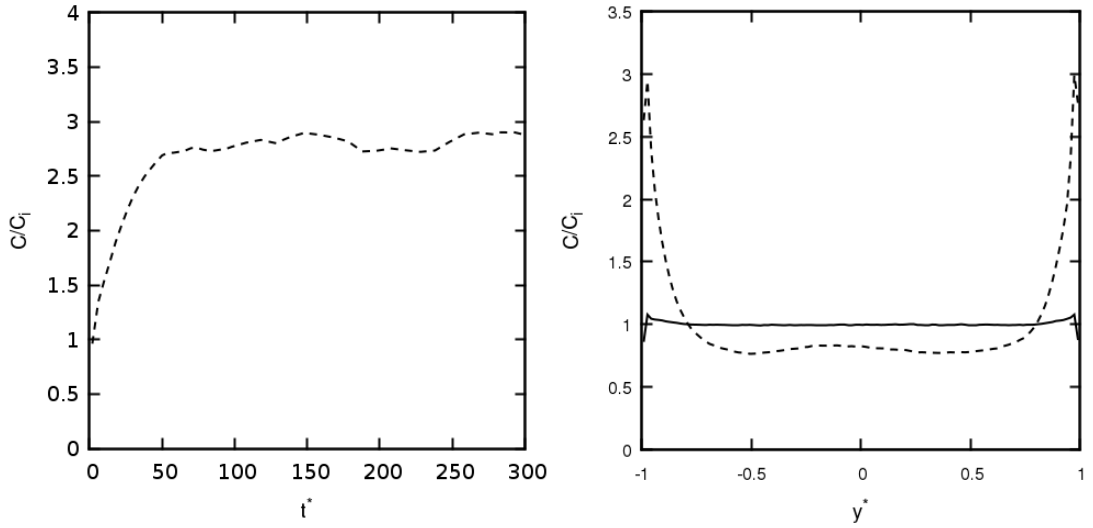

Figure 5: Instantaneous normalised particle concentration in near-wall region $y^* < 0.0083$ over time for air (left) and mean across the channel (right). —— : water; - - - : air.

Table 2: Definition of flow layers in $y^*$and particle fluxes through those regions (W: Water, A: Air).

Region	Start	End	F up (W)	F up (A)	F down (W)	F down (A)
Bulk flow	0.200	1.000	-	-	994	449
Log-law	0.166	0.200	994	456	914	458
Buffer layer	0.027	0.166	914	463	137	576
Viscous sublayer	0.000	0.027	136	576	-	-

Figure 6 overlays one-way coupled particle positions on top of contour plots of the instantaneous streamwise fluid velocity on the plane $y^* = 0.0135$ for both the air and water channel flows. It is clear that for the air channel (upper plot), the particles reside predominantly in areas of low streamwise velocity (white regions). In an effort to compare the two flows more quantitatively we define a low velocity region such that the streamwise or magnitude $(u_x^*, |\boldsymbol{u}^*| < 0.75)$ and the wall-normal and spanwise components $\left(u_y^*, u_z^* < 0.025\right)$. Figure 7 shows the percentage of time a particle spends in our definition of a low velocity region for the air and water channels. The results of this analysis are also filtered by region. Comparing the two, it is notable that in all cases particles spend more time in low velocity regions in air than they do in water. In most cases, particles in air spend almost twice as much time in these regions. Note that the percentage will be strongly dependent on where we define a low-velocity region, so the emphasis of this analysis is on comparison between the two systems.

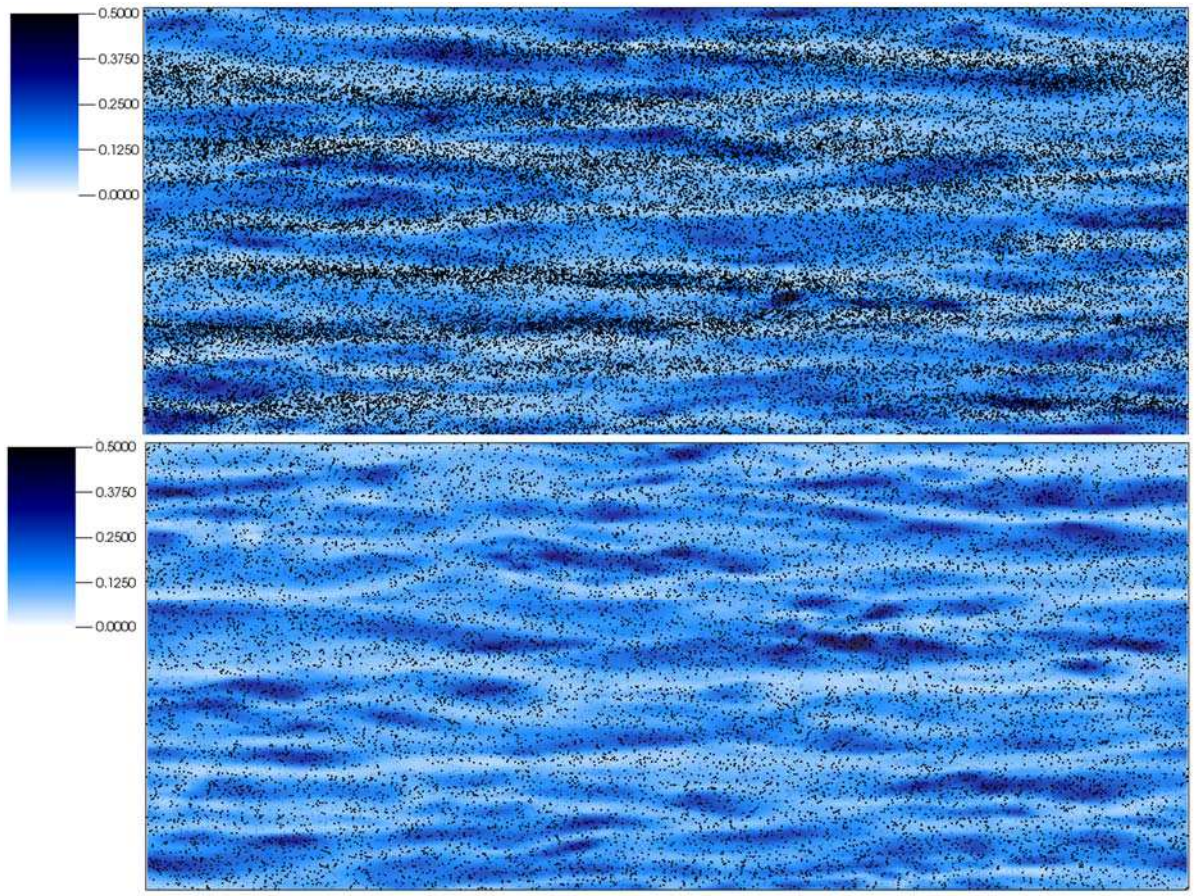

Figure 6: Particle distribution overlaid on contour plots of instantaneous fluid streamwise velocity in the viscous sublayer ($y^* = 0.0135$). Upper: Air; Lower: Water.

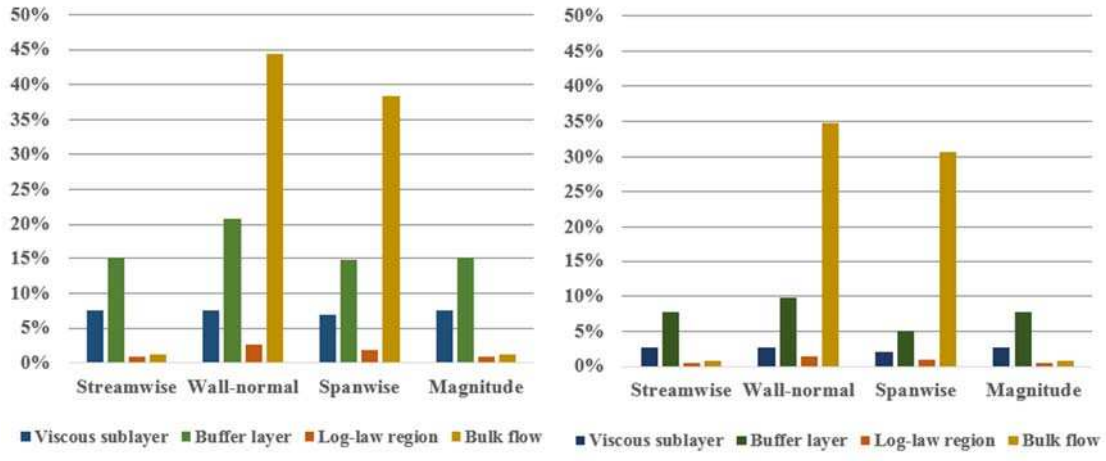

Figure 7: Percentage of time a particle spends in low velocity region for air (left) and water (right) channel flows.

4 CONCLUSIONS

This work aimed to expand the knowledge surrounding turbulence modulation and near-wall particle dynamics at high Stokes number by comparing the effects with that of a flow at low Stokes number.

It has been demonstrated that at for particles with high Stokes numbers there is a much greater impact on the turbulence, such that it dampens the streamwise component and enhances the wall-normal and spanwise components. In the near-wall region, mean particle streamwise velocity fluctuations were high for the large Stokes number system and tended to match the unladen flow for the low Stokes number system. The effect of momentum-exchange between particle and fluid and its relation to the RMS profiles for the particle phase was explored. It was speculated that the reduced fluid turbulence intensities could be due to the high particle RMS velocities in that region. It is certain that regions of high slip velocity will directly impact the magnitude of the coupling force term, but the nature of impact (attenuation or enhancement) is yet to be understood. Further work should be carried out comparing density ratios at higher particle diameters to try observe their effect on turbulence enhancement.

Particle distributions in the wall region were compared for low and high Stokes number. There was a notable increase in particle concentration near the wall during the stabilising period for the particles with greater inertia, which remained consistent for the remainder of the time considered. This was not apparent with the particles of low Stokes number, which was explained by the near identical streamwise and RMS velocity profiles. By tracing the fluid flow, the mass flux through planes in y^* must remain zero overall (as in the continuous phase), therefore there cannot be a buildup of particles in any one region. By considering particle fluxes in the wall region, we observe this to be true in the stable state for both air, and more so for water. It is also notable that the greatest amount of particle movement between one region and another takes place on the boundary between the buffer layer and the viscous sublayer for air, whereas in water this is from the bulk flow into the wall-region.

Finally, the extent to which particles remain in low velocity streaks is assessed both qualitatively and quantitively. It is indicated by considering particle distributions in the viscous sublayer that there is a tendency in air to show preference to low speed streaks, which is not apparent in water. This is confirmed and examined in further detail by partitioning the domain into regions. Results indicate that for a certain definition of a low velocity region, particles in air are around twice as likely to be found in a low speed streak than those in water. This could be further validated by considering the effect of increasing the cut-off point between ‘low’ and ‘high’ velocity regions, as particle distribution plots indicate congregation around the regions and sometimes not directly inside them.

After having observed how the turbulence is attenuated by high concentrations of small particles in high-density ratio systems, this work should be extended by performing similar simulations with larger particles. This should encourage turbulence enhancement, with the effect that density ratio and concentration has on the fluid turbulence of equal interest.

5 ACKNOWLEDGEMENTS

This work was supported by a UK Engineering and Physical Sciences Research Council grant at the University of Leeds from the EPSRC Centre for Doctoral Training in Nuclear Fission - Next Generation Nuclear.

REFERENCES

[1] Li, Y., McLaughlin, J.B., Kontomaris, K. and Portela, L. Numerical simulation of particle laden turbulent channel flow. *Phys. Fluids* (2001) **13**:2957-2967.

[2] Rouson, D.W. and Eaton, J.K. On the preferential concentration of solid particles in turbulent channel flow. *J. Fluid Mech.* (2001) **428**:149-169.

[3] Zhao, F., George, W. and Van Wachem, B. Four-way coupled simulations of small particles in turbulent channel flow: The effects of particle shape and Stokes number. *Phys. Fluids* (2015) **27**:083301.

[4] Rouson D.W.I. and Eaton, J.K. Direct numerical simulation of particles interacting with a turbulent channel flow. Proc. 7th Workshop on Two-Phase Flow Predictions, Ed. M. Sommerfeld (Erlangen, Germany, 1994).

[5] Vreman, A. Turbulence characteristics of particle-laden pipe flow, *J. Fluid Mech.* (2007) **584**:235-279.

[6] Elghobashi, S. and Truesdell, G.C. On the two-way interaction between homogeneous turbulence and dispersed solid particles. I: Turbulence modification. *Phys. Fluids* (1993) **5**:1790-1801.

[7] Fischer, P.F., Lottes, J.W. and Kerkemeier, S.G. Nek5000 Web Page. http://nek5000.mcs.anl.gov (2008).

[8] Fairweather, M. and Hurn, J.P. Validation of an anisotropic model of turbulent flows containing dispersed solid particles applied to gas-solid jets. *Comput. Chem. Eng.* (2008) **32**:590-599.

[9] Schiller, L. Neue quantitative versuche zur turbulenzentstehung. *ZAMM* (1934) **1**4:36-42.

[10] Clift, R., Grace, J.R. and Weber, M.E. *Bubbles, drops, and particles*. Courier Corporation, 2005.

[11] Saffman, P. The lift on a small sphere in a slow shear flow. *J. Fluid Mech.* (1965) **22**:385-400.

[12] Mei, R. and Klausner, J.F. Shear lift force on spherical bubbles. *Int. J. Heat Fluid Fl.* (1994) **15**:62-65.